

IL-7R α deficiency in *p53*^{null} mice exacerbates thymocyte telomere erosion and lymphomagenesis

R Kibe¹, S Zhang¹, D Guo², L Marrero¹, F Tsien^{2,3}, P Rodriguez³, S Khan¹, A Zieske⁴, J Huang⁵, W Li⁵, SK Durum⁵, T Iwakuma^{2,3} and Y Cui^{*,1,2,3}

Interleukin-7 (IL-7) is an essential T-cell survival cytokine. IL-7 receptor (IL-7R α) deficiency severely impairs T-cell development due to substantial apoptosis. We hypothesized that IL-7R α ^{null}-induced apoptosis is partially contributed by an elevated p53 activity. To investigate the genetic association of IL-7/IL-7R α signaling with the p53 pathway, we generated IL-7R α ^{null}p53^{null} (DKO) mice. DKO mice exhibited a marked reduction of apoptosis in developing T cells and an augmented thymic lymphomagenesis with telomere erosions and exacerbated chromosomal anomalies, including chromosome duplications, breaks, and translocations. In particular, Robertsonian translocations, in which telocentric chromosomes fuse at the centromeric region, and a complete loss of telomeres at the fusion site occurred frequently in DKO thymic lymphomas. Cellular and molecular investigations revealed that IL-7/IL-7R α signaling withdrawal diminished the protein synthesis of protection of telomere 1 (POT1), a subunit of telomere protective complex shelterin, leading to telomere erosion and the activation of the p53 pathway. Blockade of IL-7/IL-7R α signaling in IL-7-dependent p53^{null} cells reduced POT1 expression and caused telomere and chromosome abnormalities similar to those observed in DKO lymphomas. This study underscores a novel function of IL-7/IL-7R α during T-cell development in regulating telomere integrity via POT1 expression and provides new insights into cytokine-mediated survival signals and T-cell lymphomagenesis.

Cell Death and Differentiation (2012) 19, 1139–1151; doi:10.1038/cdd.2011.203; published online 27 January 2012

Interleukin-7 (IL-7) is an essential and nonredundant cytokine for T-cell development.¹ Humans and mice deficient in IL-7 receptor (IL-7R α) incur severe T-cell development defects, manifesting SCID.^{1–4} Early studies have shown that unbalanced survival signals of the Bcl-2 family members contribute to the impaired thymopoiesis in IL-7R α deficiency.¹ Nevertheless, ectopic expression of *Bcl-2* or inactivation of Bcl-2-associated X protein in IL-7R α ^{null} mice only partially rescues the thymopoietic defect,^{5–7} suggesting the possible involvement of the other pathways.

The tumor-suppressor p53 is a crucial transcription factor in controlling the cell cycle and apoptosis of cells under genotoxic stresses.⁸ Early studies show that p53 participates in critical thymopoiesis checkpoints related to T-cell receptor rearrangement and DNA damage repair.^{9–11} Emerging evidence suggests that p53 is a crucial regulatory factor of normal physiological processes, such as maintenance of stem cell state, development, tissue homeostasis, and autoimmunity.^{12–15} We hypothesized that p53 activation also contributes to the apoptosis and impaired thymopoiesis in IL-7R α deficiency. However, the interplay between the IL-7/IL-7R α signaling and the p53 pathway has not been demonstrated.

To decipher the potential genetic association of the IL-7R α signaling with the p53 pathway, we crossed IL-7R α ^{null} mice

with p53^{null} mice. Intriguingly, genetic deletion of p53 in IL-7R α ^{null} background (IL-7R α ^{null}p53^{null}, DKO mice) not only markedly reduced the apoptosis of developing T cells, but also significantly increased the incidence and accelerated the onset of thymic lymphoma compared with p53^{null} mice. Furthermore, p53 inactivation permitted the survival of IL-7R α ^{null} thymocytes that incurred telomere dysfunction and encouraged chromosome instability, leading to exacerbated lymphomagenesis in DKO mice. Additionally, we demonstrated that IL-7/IL-7R α signaling has a crucial role in maintaining telomere integrity and genomic stability during thymopoiesis by regulating the expression of protection of telomere 1 (POT1), a crucial component of telomere protective complex shelterin.

Results

Thymopoiesis defect in IL-7R α ^{null} mice is associated with a marked increased in p53 activity. IL-7R α deficiency results in a 99% to 99.9% reduction in thymic cellularity.⁴ Besides the documented imbalance of pro-survival and pro-apoptotic signals of the Bcl-2 family members,^{4–7} we postulated that elevated p53 activity also contributes to the

¹Louisiana State University Health Sciences Center, Gene Therapy Program, 533 Bolivar Street, New Orleans, LA 70112, USA; ²Department of Genetics, 533 Bolivar Street, New Orleans, LA 70112, USA; ³Department of Stanley Scott Cancer Center, 533 Bolivar Street, New Orleans, LA 70112, USA; ⁴Department of Pathology, 533 Bolivar Street, New Orleans, LA 70112, USA and ⁵Section of Cytokines and Immunity, National Cancer Institute, Frederick, MD 21702, USA

*Corresponding author: Y Cui, Louisiana State University Health Sciences Center, 533 Bolivar Street, New Orleans, LA 70112, USA. Tel: +1 504 568 4636;

Fax: +1 504 568 8500; E-mail: ycui@lsuhsc.edu

Keywords: IL-7R α ; p53; telomere dysfunction; genomic instability; lymphomagenesis

Abbreviations: IL-7R α , IL-7 receptor α chain; POT1, protection of telomere 1; DN, CD4⁺CD8⁺ double negative; DP, CD4⁺CD8⁺ double positive; ISP, CD4⁺CD8⁺ immature single positive; SKY, spectral karyotyping; Telo-FISH, telomeric fluorescence *in situ* hybridization; Flow-FISH, flow cytometry-based analysis of Telo-FISH; TIF, telomere-induced DNA damage foci; IF-FISH, immunofluorescent fluorescence *in situ* hybridization; TRF, terminal restriction fragment

Received 12.7.11; revised 12.12.11; accepted 12.12.11; Edited by JC Marine; published online 27.1.12

thymopoietic defect in *IL-7R α ^{null}* mice. Our immunofluorescence staining for p53 confirmed a preferential increase in the percentage of p53-positive thymocytes in *IL-7R α ^{null}* mice as compared with those in wild-type (WT) and *p53^{null}* mice (Figure 1a). Because p53 phosphorylation is associated with its activation,¹⁶ we determined its levels. Indeed, phosphorylation of p53 at serines 23 (p53Ser²³) and 18 (p53Ser¹⁸) in the thymocytes of *IL-7R α ^{null}* mice was markedly increased as compared with those of WT and *p53^{null}* mice (Figure 1b). This enhanced p53 activity in *IL-7R α ^{null}* thymocytes was confirmed as marked upregulation of p53 downstream targets, such as p53 upregulated modulator of apoptosis (puma) and p21, by western blotting and quantitative RT-PCR (Figures 1b and c). Similarly, an increase in Bcl-2-associated X protein mRNA with a concurrent reduction in Bcl2 mRNA in *IL-7R α ^{null}* thymocytes was also observed (Figure 1c). To determine the thymocyte subsets that incurred elevated p53 activity, we employed

intracellular staining of p53Ser¹⁸ and found that CD4⁻8⁻ subpopulation of both WT and *IL-7R α ^{null}* mice sustained the highest level of p53Ser¹⁸ staining (Supplementary Figure S1A). Some CD4⁺ and CD8⁺ thymocytes of *IL-7R α ^{null}* mice also incurred elevated p53Ser¹⁸ activity (Supplementary Figure S1A). Consistent with a previous report,⁹ p53 was not activated in the thymi of *Rag1^{null}* mice whose impaired thymopoiesis was caused by a failure to initiate T-cell receptor rearrangement (Supplementary Figure S1B). Together, these results suggest that the activated p53 pathway is a specific contributing factor to the impaired thymopoiesis in *IL-7R α ^{null}* mice.

Genetic inactivation of p53 reduces the apoptosis of developing thymocytes in *IL-7R α ^{null}* mice with a dire consequence of augmented thymic lymphomagenesis. To explore whether genetic deletion of *p53* in *IL-7R α ^{null}* mice prevents apoptosis and restores thymopoiesis,

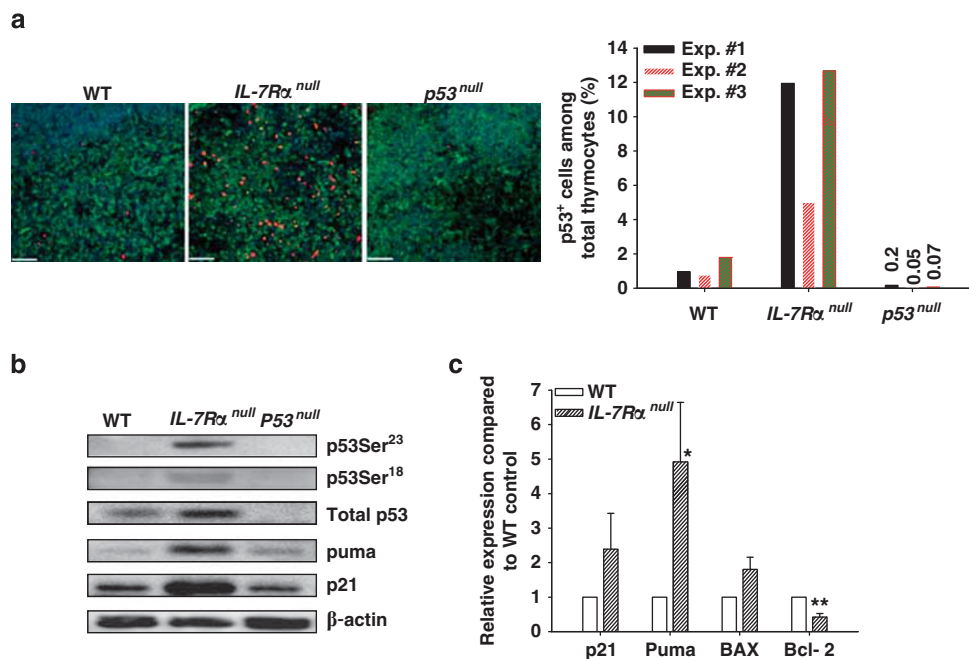
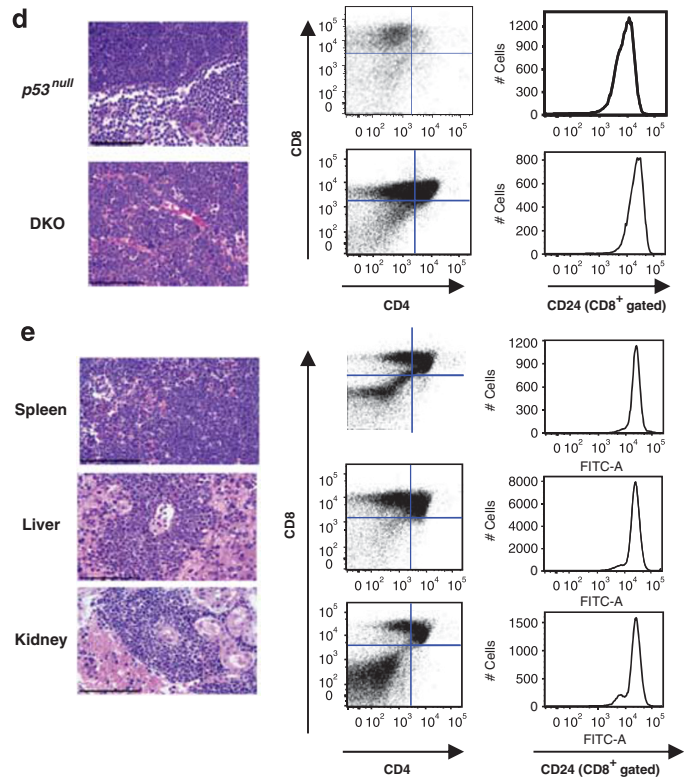
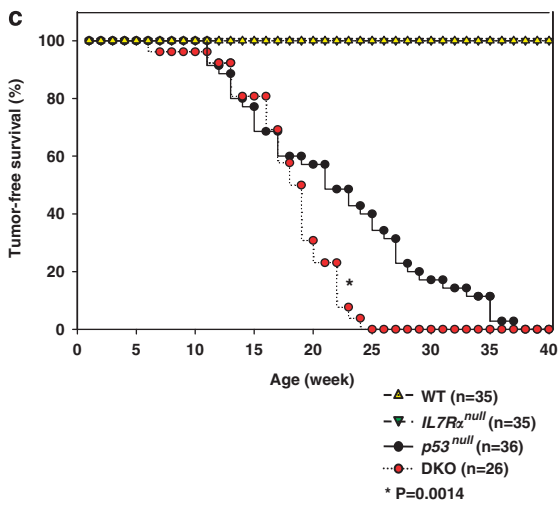
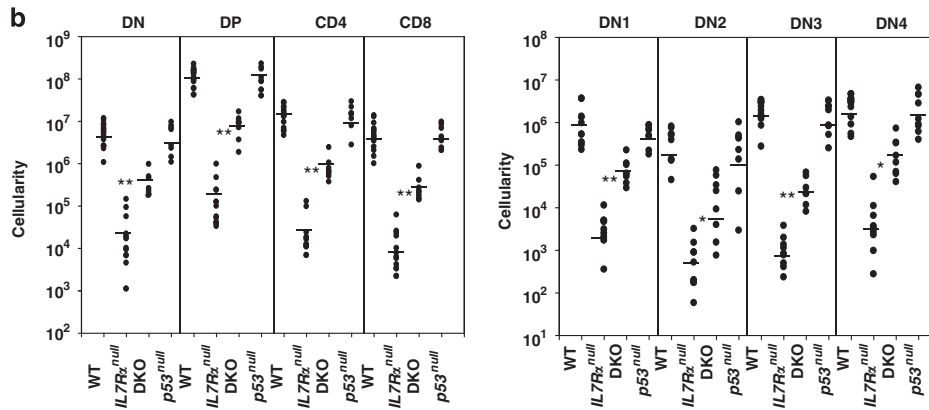
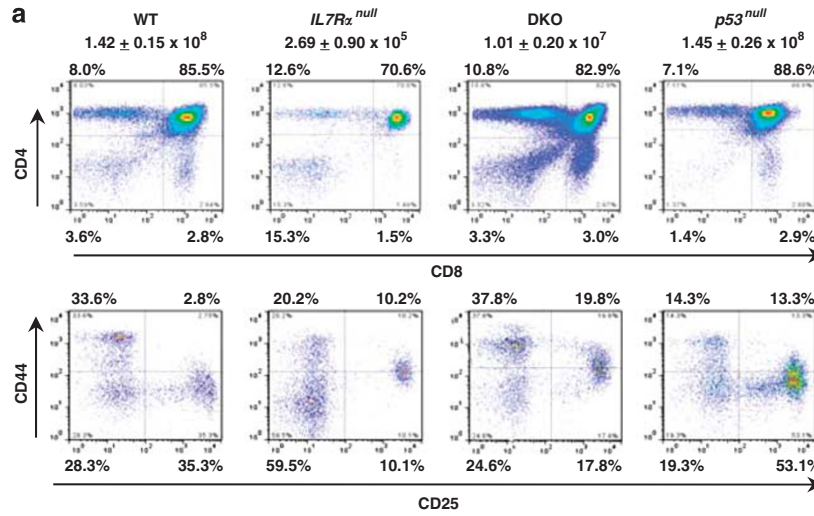


Figure 1 Thymopoiesis defect in *IL-7R α ^{null}* mice is associated with a marked increase in p53 activity. Thymi of 4–8 week-old WT, *IL-7R α ^{null}*, and *p53^{null}* mice were used to examine p53 activity. (a) Representative images of immunofluorescence staining of p53-positive thymocytes (red, clone CM5; Novocastra) in both CD3⁺ (green) and CD3⁻ thymocytes (scale bars = 50 μ m) (left panel). Percentage of p53-positive thymocytes from three independent experiments is presented on the right. (b) Total p53, phosphorylated p53 at serines 23 and 18, and p53 downstream targets puma and p21 in thymocyte lysate were examined by Western blotting (WB). (c) RNA expression level of pro-apoptotic and anti-apoptotic genes, including those of p53 downstream targets, was determined via real-time RT-PCR. Data are presented as mean \pm s.e. of 3–5 mice/group. * and ** denote significant difference, $P < 0.05$ and $P < 0.01$, respectively, unpaired Student's *t*-test. Experiments in (b) and (c) were repeated at least three times with pooled thymocytes from up to 10 *IL-7R α ^{null}* mice/experiment

Figure 2 Genetic inactivation of *p53* in *IL-7R α ^{null}* mice partially restores thymocyte development at the expense of exacerbated thymic lymphomas with systemic dissemination. (a) and (b) Fresh thymocytes of 4–6-week-old WT, *IL-7R α ^{null}*, DKO, and *p53^{null}* mice were harvested to determine the total number of viable thymocytes and frequency of each subpopulation. (a) Representative FACS analyses of thymocyte composition of CD4⁺8⁻, CD4⁺8⁺ (DP), CD4⁻8⁻ (DN), and CD4⁻8⁺ subpopulations, as well as CD44⁺25⁻ (DN1), CD44⁺25⁺ (DN2), CD44⁻25⁺ (DN3), and CD44⁻25⁻ (DN4) cells among the DN subpopulation. The cellularity of total thymocytes is presented as mean \pm s.e. of 8–18 mice/genotype. (b). The number of each subpopulation in individual mouse of various genotypes is plotted as a dot and the mean among each group is presented as a bar. *Represents the significance of $P < 0.05$, whereas **denotes a significance of $P < 0.001$, when comparing the number between age-matched *IL-7R α ^{null}* and DKO mice. (c) Survival of cohorts of WT, *IL-7R α ^{null}*, DKO, and *p53^{null}* mice during a 40-week period is depicted (*n* represents the number of mice, $P < 0.01$, log-rank test). (d) Thymic lymphomas developed in *p53^{null}* and DKO mice were examined. Representative H&E staining of thymic lymphomas developed in *p53^{null}* and DKO mice. Cell surface marker expression of *p53^{null}* and DKO thymic lymphomas was compared via FACS. (e) Tumor disseminations in DKO mice that developed thymic lymphomas were examined. Representative H&E staining (left panels) and cell-surface marker expression of disseminated tumors (right panels) in the spleen, liver, and kidney of DKO mice show similar phenotype to those in DKO thymi. Data in (d) and (e) are representative of at least five independent experiments. Scale bars = 100 μ m



we generated DKO mice by crossing IL-7R α ^{null} and p53^{null} mice in the C57BL/6 background. As expected, the thymocyte composition of CD4⁺8⁻, CD4⁺8⁺ (DP), CD4⁻8⁻, and CD4⁻8⁺ subpopulations in DKO mice was largely restored to a comparable level to that of WT thymocytes with a more than 30-fold increase in thymic cellularity (Figure 2a). The cellularity of all four pro-T subsets, DN1 to DN4, was markedly increased in DKO mice, although those of CD44⁺25⁻ (DN1) and CD44⁻25⁺ (DN3) were more profound (Figure 2b). Because all p53^{null} mice succumbed to tumorigenesis and died within 40 weeks with a median survival of 23 weeks (Figure 2c),¹⁷ we explored whether IL-7R α ^{null} imposed any effects on T-cell lymphomagenesis of the p53^{null} background by monitoring cohorts of WT, IL-7R α ^{null}, p53^{null}, and DKO mice for 40 weeks. Strikingly, DKO mice developed tumors significantly earlier than p53^{null} mice with 100% mortality by 25 weeks and a median survival of 18 weeks (Figure 2c). Neither WT nor IL-7R α ^{null} mice developed tumors during this period (Figure 2c). Pathological and flow cytometry (FACS) examinations revealed that more than 80% of the DKO mice, as compared with 42% of the p53^{null} mice, developed thymic lymphomas (Supplementary Table 1). These thymic lymphomas from both DKO and p53^{null} mice appeared to similarly arise from immature CD4⁺CD8⁺CD24⁺ISP and CD4⁺CD8⁺CD24⁺DP thymocytes (Figure 2d). Interestingly, close to 60% of thymic lymphomas in DKO mice disseminated systemically to both lymphoid, such as the spleen and lymph nodes, and non-lymphoid tissues, such as the liver and kidneys, whereas only 13% of the tumors from p53^{null} mice showed limited dissemination to the lymphoid but not non-lymphoid tissues (Figure 2e and Supplementary Table 2). FACS analysis further confirmed thymic origin of the disseminated tumors in DKO mice (Figure 2e). These results clearly demonstrate that inactivation of p53 partially, but markedly, restored the thymopoiesis defects of IL-7R α ^{null} with the dire consequence of augmented thymic lymphomagenesis. Our study provides direct evidence of the functional interplay between IL-7R α signaling and the p53 pathway during thymopoiesis.

Thymic lymphomas in DKO mice incur exacerbated genomic instability. Genomic instability, such as aneuploidy and translocation, is a hallmark and potential cause of tumorigenesis.^{18,19} To investigate whether the augmented lymphomagenesis and enhanced dissemination in DKO mice were associated with increased genomic instability, we performed DNA content analysis via FACS. Fresh thymic lymphomas from p53^{null} mice contained aneuploid and polyploid (>4n, Figure 3a) cells, similar to previous observations,^{20,21} whereas the frequency of irregular DNA contents was greatly increased in DKO thymic lymphomas (Figure 3a). Moreover, within each tumor sample, a significantly higher percentage of polyploidy was observed in DKO tumors (Figure 3b, DKO versus p53^{null}, $P=0.017$, two-tailed Mann-Whitney rank sum test). Cytogenetic analyses with thymic lymphomas from eight DKO and four p53^{null} mice further confirmed exacerbated genomic instability in DKO tumors: 30% of 50 metaphases examined from the DKO lymphomas maintained diploid chromosome number of 40 (=2n), whereas more than

65% of the 50 metaphases from p53^{null} tumors showed diploid chromosome number (Figure 4a). More strikingly, over 80% metaphases from DKO tumors contained at least one translocation involving centromeric fusions between the telocentric chromosomes (Robertsonian translocation), among which approximately 40% contained 2–4 translocations/cell (Figure 4b). In sharp contrast, translocations in tumors from p53^{null} mice were very rare and none of the metaphases contained two or more translocations per cell (Figure 4b), similar to previous reports.^{20,21} To further explore other chromosome aberrations in the thymic lymphomas, we employed spectral karyotyping (SKY) analyses. Indeed, DKO tumors frequently showed unbalanced near-triploid chromosome amplification, besides chromosome breaks and non-clonal unbalanced translocations (Figure 4c and Supplementary Table 3), whereas chromosome structural aberrations were rarely observed in p53^{null} tumors (Supplementary Figure S2).^{20,21} To determine whether chromosome instability is observed prior to tumor development, we karyotyped thymocytes from 4–6-week-old DKO mice before overdevelopment of tumors, defined as aberrant ISP and DP composition via FACS. Indeed, chromosome duplications and fusions were observed in these pre-malignant DKO thymocytes (Supplementary Figure S3A), indicating that chromosome instability preceded overdevelopment of tumor. To further confirm their lack of early emerging lymphomas, thymocytes of 4–6-week-old DKO mice were also transferred to syngeneic Rag^{null} mice that lacked mature T cells. CD4⁺ and CD8⁺ mature T cells were observed in the peripheral blood lymphocytes of Rag^{null} mice that received DKO thymocytes over the 3-month period of observation (Supplementary Figure S3B). These transferred thymocytes did not develop into lymphomas in Rag^{null} mice, like those of ISP or DP phenotypes in the spleen and thymus of DKO mice (Supplementary Figure S3C and Figures 2d and e). Together, these results confirm that genomic abnormality occurred in pre-malignant DKO thymocytes and strongly support the notion that IL-7R α deficiency in combination with p53 deficiency permits the survival of developing thymocytes and encourages genomic instability, thereby exacerbating lymphomagenesis.

IL-7R α ^{null} deficiency is associated with telomere dysfunction, which activates DNA damage signals that coincide with telomere signals. Chromosome translocations and fusions can be triggered by various mechanisms, such as T-cell receptor rearrangement, DNA damage-induced double-strand DNA breaks, telomere dysfunction, and DNA repair defects.^{10,18,20,22,23} Robertsonian translocations frequently occur in cells incurring telomere dysfunction.^{22,24} We, therefore, hypothesized that IL-7R α ^{null} results in telomere dysfunction leading to the exacerbated lymphomagenesis in DKO mice. Telomeric fluorescence *in situ* hybridization (Telo-FISH) revealed complete loss of telomeres at the centromeric fusions of all Robertsonian translocations and some of non-fused chromosomes in DKO lymphomas (Figure 5a), whereas no obvious telomere loss was observed in p53^{null} tumors (Figure 5a). Telo-FISH analyses with fresh unmanipulated thymocytes from 4–6-week-old DKO and p53^{null} mice

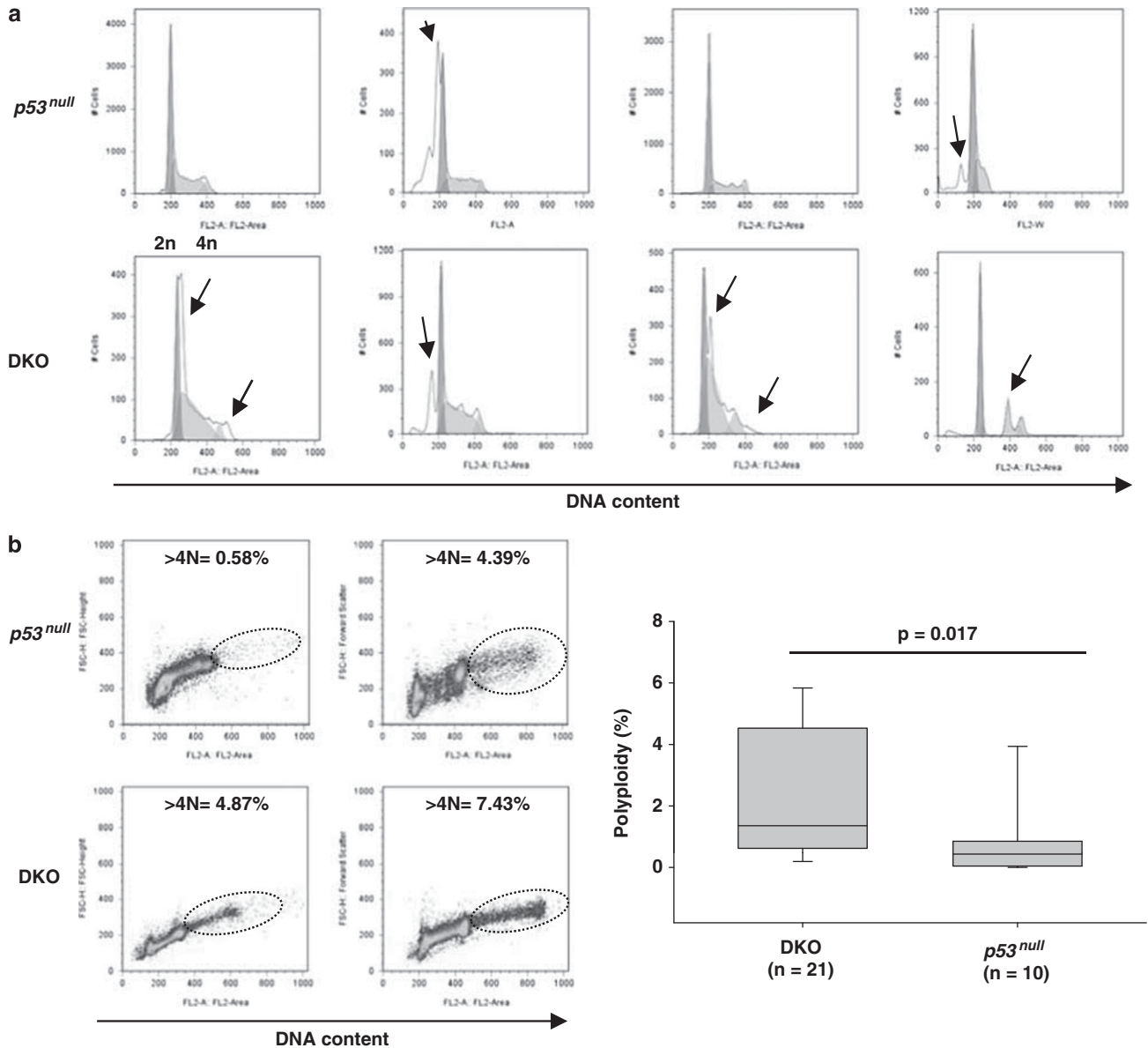


Figure 3 Accelerated thymic lymphomagenesis in DKO mice is associated with exacerbated genomic instability. Fresh thymic lymphomas harvested from DKO and *p53*^{null} mice were examined for aberrant DNA content via FACS. **(a and b)** Representative FACS analyses of DNA content of thymic lymphomas from DKO and *p53*^{null} mice are presented to reveal aneuploidy **(a, arrows)** and polyplody **(b, dashed ovals)**; the percentage of polyplody (> G2/M) thymic lymphomas from 21 DKO and 10 *p53*^{null} mice was determined via FACS. Differences between the two groups were compared (two-tailed Mann–Whitney rank sum test, *P* = 0.017). The line within each box represents group median, whereas the upper and lower box boundaries mark the 25th and 75th percentiles, and error bars represent the 10th and 90th percentiles

confirmed that telomere dysfunction occurred in pre-malignant DKO thymocytes as multi-telomere loss (up to 3/metaphase) in about 27% thymocytes examined as compared with the occasional (7%) undetectable telomeres (not > 1/metaphase) in *p53*^{null} thymocytes (Figure 5b). Likewise, Telo-FISH analysis on fresh *IL-7R α* ^{null} thymocytes also confirmed the frequent loss of telomeres and an overall reduction in the intensity of telomere hybridization signals (Supplementary Figure S4). Because of the difficulty in obtaining sufficient number of metaphases from *IL-7R α* ^{null} thymocytes, we employed a flow cytometry-based analysis of Telo-FISH signal (Flow-FISH) to determine the mean fluorescence intensity of telomere signals of cells that possessed identical DNA content

determined by propidium iodide staining. As shown in Figure 5c, Flow-FISH analyses confirmed that telomere signals of *IL-7R α* ^{null} and DKO thymocytes were significantly reduced compared with those of WT and *p53*^{null} thymocytes with identical DNA content of 2n, which were G₀/G₁ phase cells. These results demonstrate that developing thymocytes fail to maintain telomere integrity in the absence of IL-7R α .

Telomere dysfunction, either via telomere uncapping or shortening, is sensed as double-strand DNA breaks, which trigger DNA damage responses and activate the checkpoint pathways.^{19,25–27} Consequently, these lead to the localization of DNA damage response factors, such as γ H2AX and 53BP1, at the site of dysfunctional telomeres called telomere-induced

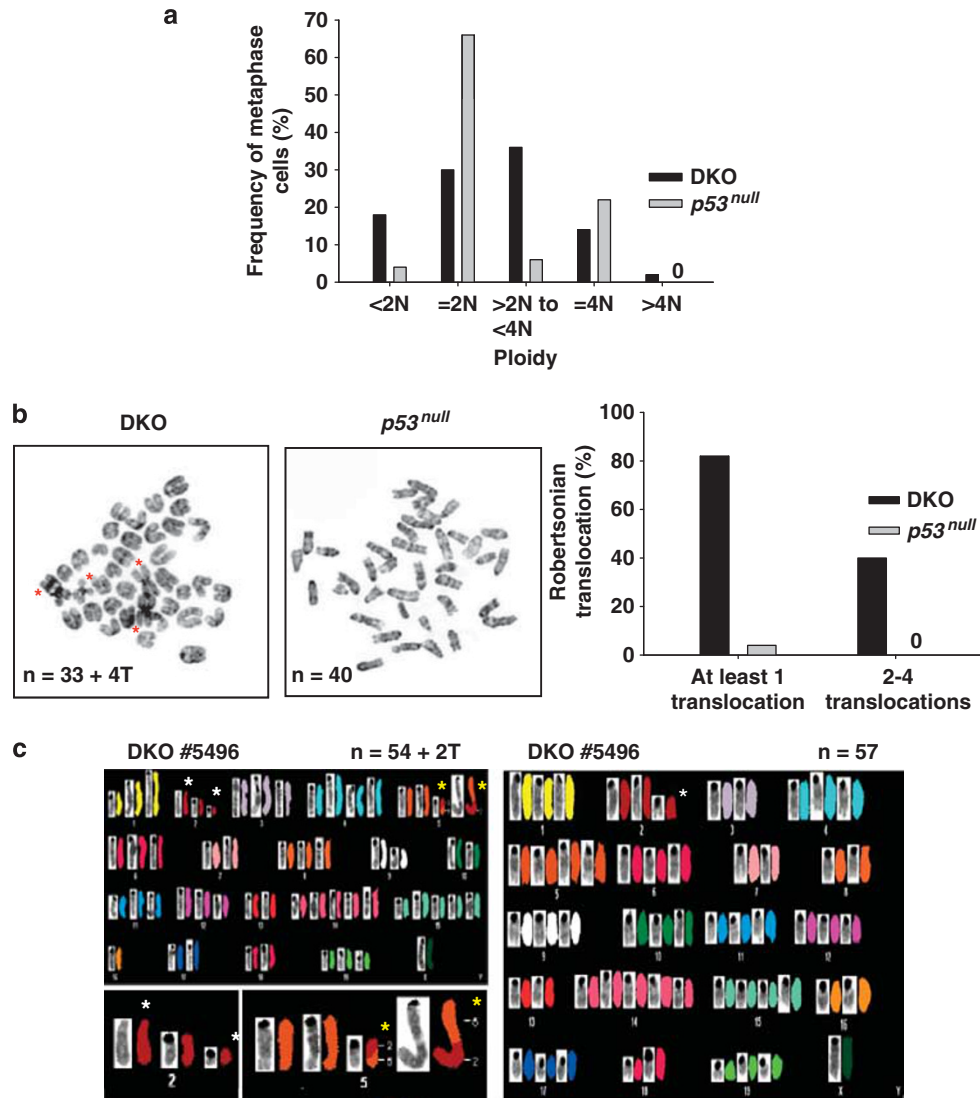


Figure 4 Genomic instability in DKO thymic lymphomas is further exemplified by marked chromosomal numerical and structural aberrations. Fresh thymic lymphomas harvested from DKO and *p53*^{null} mice were prepared for cytogenetic analyses. (a) Frequency of diploidy (2n), tetraploidy (4n), and aneuploidy (<2n, >2n to <4n, and >4n) among 50 metaphases from eight DKO tumors and 50 metaphases from four *p53*^{null} tumors was analyzed and summarized. (b) Representative G-band karyotyping images of metaphase preparation reveal Robertsonian translocations, that is, chromosome centromeric fusions (red asterisks), in DKO tumors (left panels). Images were captured using an Applied Imaging ER-3339 cooled CCD camera (ASI) mounted on top of a Nikon Eclipse E400 with CytoVision 3.1 software (ASI). *n* denotes the total chromosome number, whereas T indicates Robertsonian translocations. The frequency of Robertsonian translocations observed among the 50 metaphases of each tumor type was summarized in the right panel. Each experiment is repeated at least five times involving 5–8 tumors of each genotype. (c) Representative SKY images of DKO lymphoma illustrate numerical and structural anomalies of the chromosomes associated with unbalanced chromosome amplification, breaks (white asterisks), and fusions (yellow asterisks). Images were acquired using a SD301 SpectraCube™ system (ASI) mounted on top of an epifluorescence microscope Axioplan 2 (Zeiss) and analyzed using Spectral Imaging 4.0 acquisition software (ASI). G banding was simulated by electronic inversion of DAPI counterstaining

DNA damage foci (TIF).^{25,27,28} To validate the effects of *IL-7R α* ^{null} in inducing telomere dysfunction, we examined TIFs in *IL-7R α* ^{null} and DKO thymocytes by immunofluorescence staining of γ H2AX followed by Telo-FISH (immunofluorescent fluorescence *in situ* hybridization (IF-FISH)). Confocal microscopic image analyses of >50 thymocytes from each genotype revealed that over 70% of *IL-7R α* ^{null} and DKO thymocytes incurred >4 TIF/cell, whereas only 15–30% of WT and *p53*^{null} thymocytes contained >4 TIF/cell (Figure 5d). In contrast, irradiated WT thymocytes did not show distinct TIFs despite a massive upregulation of γ H2AX induced by the

irradiation (Supplementary Figure S5). Among the thymocytes examined, not all DNA damage signals colocalized with telomeres, suggesting the existence of other DNA damages during thymopoiesis (Figure 5d). To verify that IL-7/IL-7R α signaling withdrawal caused the increases in TIF, we performed IF-FISH analysis using an established IL-7-dependent *p53*^{null} thymic cell line D1Bcl2 that was resistant to apoptosis because of constitutive expression of Bcl2.^{29,30} IL-7 withdrawal from D1Bcl2 cells resulted in cell cycle arrest within 24 h without apparent induction of apoptosis up to 72 h.³⁰ However, it greatly enhanced the DNA damage signals

revealed by co-staining with anti- γ H2AX and 53BP1 antibodies, the majority of which also colocalized with telomeres as TIFs (Figure 5e). Together, these results strongly suggest that the lack of IL-7/IL-7R α signaling in developing thymocytes leads to telomere dysfunction, which triggers DNA damage responses, activates the p53 pathway, and induces apoptosis. Genetic deletion of *p53* allows the survival of those thymocytes-accruing telomere dysfunction, DNA damages, and chromosome abnormalities, which initiate and mark the early transition towards tumorigenesis.

IL-7 signaling blockade in *p53^{null}* D1 cell line recapitulates telomere dysfunction and chromosomal anomalies observed in DKO lymphomas. To recapitulate our *in vivo* results of the telomere dysfunction and genomic instability observed in DKO thymocytes, we analyzed telomere signals at various time points after IL-7 withdrawal from D1 cells via Flow-FISH. As expected, IL-7 withdrawal resulted in a significant reduction (~25%) in telomere signal at as early as 16 h (Figure 6a). At 20–24 h after IL-7 withdrawal, the telomere signal was reduced by about 50%, leading to a complete loss of telomere signal and apoptosis by 30–40 h (Figure 6a). To verify that the observed drastic reduction in telomere signals via Flow-FISH reflected telomere shortening, we assessed telomere length by Southern blot analysis of terminal restriction fragments (TRFs) (Figure 6b). Similar to Flow-FISH results, IL-7 withdrawal from D1 cells resulted in a reduction of telomere length to 18.3 Kb within 16 h from 32 Kb and a further decrease to 12.7 Kb by 20 h post-IL-7 withdrawal (Figure 6b). Together, these results confirm that IL-7 withdrawal results in telomere erosion and genomic instability in IL-7-dependent thymocytes.

As IL-7 withdrawal from D1 cells induced rapid apoptosis in 30–40 h, which prevented us from examining chromosome abnormalities induced by gradual or partial IL-7 withdrawal (Supplementary Figure S6A), we explored whether an appropriate dose of a JAK3 inhibitor could block D1 proliferation with minimal induction of apoptosis. JAK3 inhibitor VI blocked the IL-7-mediated proliferation at 2 μ M without inducing massive apoptosis during the first 40 h (Supplementary Figure S6). DNA content analyses revealed that the JAK3 inhibitor treatment induced a G₂/M phase cell cycle arrest and a marked increase in polyploidy (>4n) to 10–20% as compared with a <0.5% polyploidy in untreated D1 cells (Figure 6c). Further examination on chromosome integrity via karyotyping and Telo-FISH confirmed that 10–20% of the cells became polyploid, possessing diplo- and quadruple-chromosomes by 40 h of the JAK3 inhibitor treatment (Figures 6d and e). Strikingly, this observed chromosome numerical abnormality was also associated with telomere attrition, chromosome breaks, Robertsonian translocations (Figure 6e, inserts), and reminiscence of the abnormalities observed in our DKO thymic lymphomas. Altogether, these results strongly support the notion that IL-7R α deficiency results in telomere dysfunction, which leads to chromosome abnormalities in *p53^{null}* cells.

IL-7/IL-7R α signaling protects telomeres by maintaining protein synthesis of POT1. Telomeres are protected by a specialized protein complex shelterin, consisting of TRF1 (telomeric repeat binding factor 1 or TERF1),

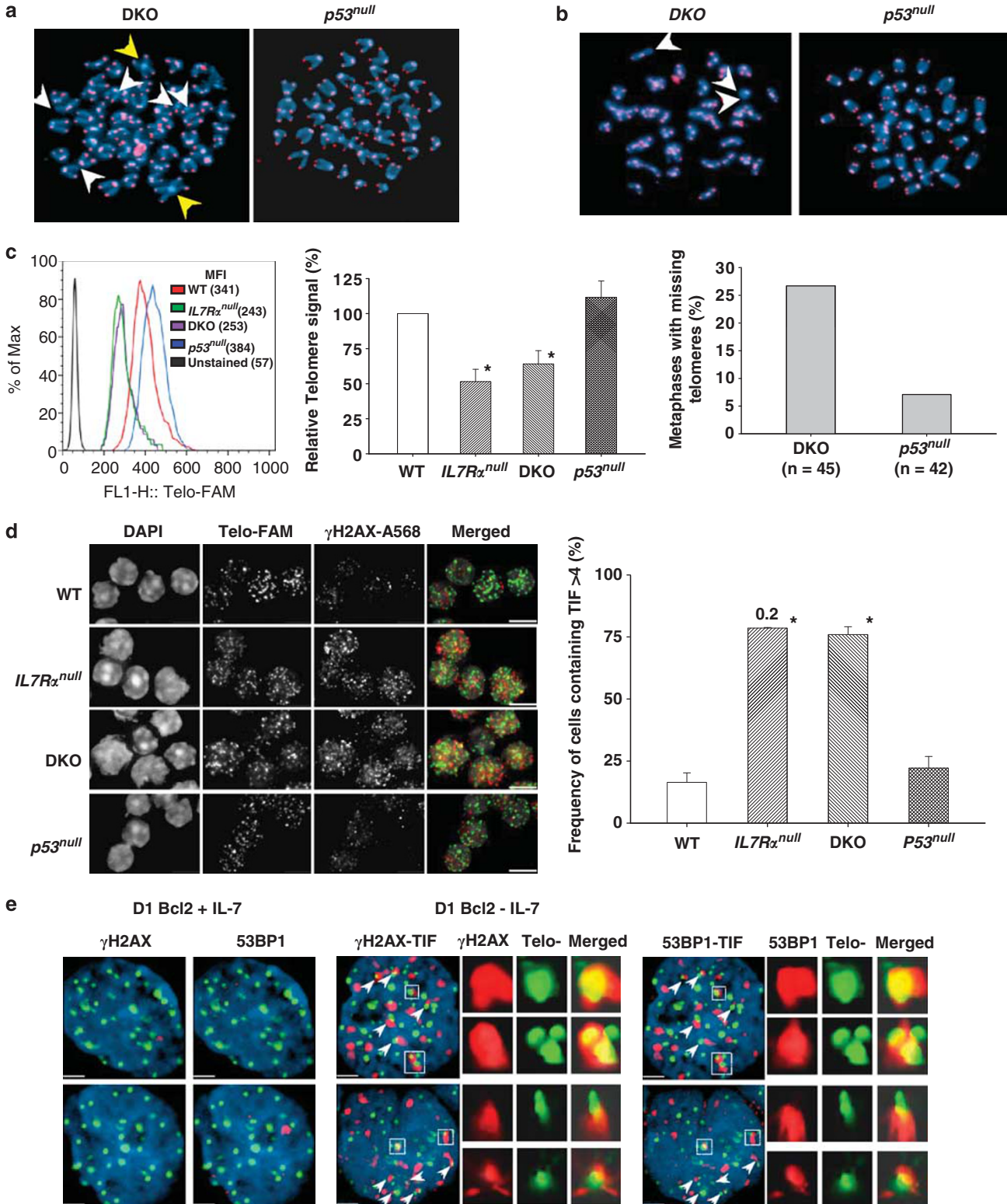
TRF2, TIN2 (TERF1-interacting nuclear factor 2), TPP1 (or adrenocortical dysplasia protein homolog), repressor activator protein 1, and POT1.²⁶ Deficiency in either TRF2 or POT1, which binds double-strand or single-strand telomeric DNA, respectively, induces telomere dysfunction that activates DNA damage signals and the p53 pathway.^{26,31,32} Therefore, we explored the effects of IL-7 withdrawal from D1 cells on shelterin subunits. Intriguingly, at 20 h post-IL-7 withdrawal, POT1 protein expression was greatly diminished, associated with an elevated γ H2AX (Figure 7a). The level of TPP1 was modestly reduced. However, the expression of other shelterin subunits TFR1, TRF2, and TIN2 was unaffected by the IL-7 withdrawal (Figure 7a). Similar reduction of POT1 expression also occurred *in vivo* in *IL-7R α ^{null}* thymocytes as compared with that of WT thymocytes (Figure 7b). Only modest reduction in the expression of TPP1, TRF2, and TIN2 was observed, whereas that of TRF1 and repressor activator protein 1 was unaffected in *IL-7R α ^{null}* thymocytes (Figure 7b). Further, kinetic analyses upon IL-7 withdrawal demonstrated an inverse correlation between the levels of POT1 and γ H2AX in D1 cells (Figure 7c). Similarly, the Jak3 inhibitor greatly suppressed IL-7-mediated STAT5 phosphorylation and POT1 expression, but not that of TIN2, with a concomitant increase in γ H2AX (Figure 7d). These results strongly suggest that IL-7/IL-7R α signaling is essential for proper POT1 expression and the maintenance of telomere integrity in IL-7-dependent cells.

To better understand the regulatory mechanism of POT1 by IL-7, we examined the mRNA levels of both POT1a and POT1b, two murine orthologs, in D1 cells upon IL-7 withdrawal and found that neither RNA transcript was affected (Supplementary Figure S7). As POT1a and POT1b proteins have an identical molecular size and the antibody we used does not distinguish these two proteins, our analyses on POT1 protein were not meant to discriminate them. We examined whether POT1 protein stability was affected by the IL-7/IL-7R α signaling in D1 cells in the presence of a protein synthesis inhibitor cycloheximide. However, the presence or absence of IL-7 did not alter the kinetics of POT1 degradation in D1 cells (Supplementary Figure S8), suggesting that IL-7 signaling did not regulate POT1 protein stability. To further determine whether POT1 protein synthesis was altered in the absence of IL-7, we performed metabolic labeling upon IL-7 withdrawal and found that the level of newly synthesized POT1, measured by the ³⁵S-Methionine labeling, was greatly diminished within 12 h of IL-7 withdrawal (Figure 7E), indicating that IL-7 regulates POT1 at the protein synthesis level. Finally, to test whether enforced expression of either POT1a or POT1b would rescue the telomere attrition by IL-7 withdrawal in D1 cells, we subjected D1Bcl2 cells overexpressing POT1a or POT1b to IL-7 withdrawal. Interestingly, either POT1a or POT1b alone did not prevent IL-7 withdrawal-induced telomere attrition, but co-expression of POT1a and POT1b prevented the telomere loss induced by IL-7 withdrawal (Figure 7F). Taken together, these results strongly suggest that IL-7/IL-7R α signaling protects telomere integrity by maintaining POT1 expression at the protein synthesis level in both IL-7-dependent D1 cells and primary thymocytes.

Discussion

Our study reveals a previously unappreciated interaction between IL-7/IL-7R α signaling and the p53 pathway, as well as the crucial role of IL-7/IL-7R α in maintaining genomic

stability during thymopoiesis. We demonstrate that in the absence of IL-7/IL7R α signaling, IL-7-dependent cells fail to maintain POT1 protein synthesis and telomere integrity, leading to rapid telomere attrition, activation of DNA damage



signal, and activation of the p53 pathway. Genetic deletion of *p53* in *IL-7R α* ^{nu/nu} background permits the survival of thymocytes-accurring telomere dysfunction, but encourages chromosome instability and exacerbates lymphomagenesis. Our results clearly demonstrate that activation of the p53 pathway is another contributing pro-apoptotic signal in *IL-7R α* ^{nu/nu} thymocytes, besides the well-documented unbalanced signals of the Bcl-2 family members.^{1,4} Therefore, multiple pro-survival pathways are involved in the essential and nonredundant function of IL-7/IL-7R α signaling during T-cell development.

Recent evidence demonstrates that POT1 is essential for protecting telomeres from rapid degradation.^{31–33} Our study is the first that demonstrates the essential role of POT1 in cytokine-mediated T-cell development by suppressing telomeric DNA damage signals. Although the consequence of *POT1*^{nu/nu} to T-cell development is not previously documented because of embryonic lethality of *POT1a*^{nu/nu} mice, the observed chromosome abnormalities in our DKO thymic lymphomas are similar to those reported in mouse embryonic fibroblasts lacking *POT1a/b*, especially those with simultaneous inactivation of *p53*.^{32,33} Our results with ectopic expression of POT1a/b in D1 cells and those of the above-referenced reports of *POT1a/b*^{nu/nu} mouse embryonic fibroblast strongly suggest that both POT1a and POT1b are required to prevent telomeric DNA damage signals and the loss of both promotes polyploidy, chromosome fusions, and breaks.^{32,33} Moreover, our study also suggests that IL-7 regulates POT1 expression at the protein synthesis level via the JAK3-STAT5 pathway because JAK3 inhibitor treatment of D1 cells suppresses POT1 expression and mimics chromosome abnormalities incurred in DKO lymphomas. This notion also agrees with a previous report on JAK3 inhibitor-induced endoreduplication in leukemia cells.³⁴ Nevertheless, IL-7 deficiency-induced telomere dysfunction as rapid telomere erosion in D1 cells, and *IL-7R α* ^{nu/nu} and DKO thymocytes was not reported in *POT1a/b*^{nu/nu} mouse embryonic fibroblast.^{32,33} The differences between our study and previous observations are likely related to the cellular context, that is, intrinsic properties of different cell type and the potential contribution of other IL-7-dependent effects, which will be investigated in future studies.

Recent observations reveal that about 10% T-cell acute lymphoblastic leukemia carry gain-of-function mutations of *IL-7R α* gene, which promote oncogenic transformation via constitutive activation of JAK1, but not JAK3.^{35,36} Nevertheless, this T-cell acute lymphoblastic leukemia is not linked to poor prognosis,^{35,36} suggesting a different tumorigenic process from that of our DKO mice. As IL-7R α deficiency causes lymphopenia, which was modestly improved in DKO mice by *p53* inactivation but to a lesser extent than that by Bcl2 overexpression,^{5–7} it is also plausible to propose that the lymphopenia environment promotes vigorous compensatory proliferation of stem cells and progenitors, and encourages accrued mutations and genomic instability, thereby enhancing their risk of oncogenesis like those observed in recent studies.^{37,38} Therefore, IL-7 signaling should be exquisitely controlled to ensure proper thymopoiesis while preventing lymphomagenesis.

In summary, this is the first study illustrating the functional interplay of the IL-7R α signaling with the p53 pathway in maintaining genomic stability during thymopoiesis. Our study underscores a novel function of IL-7R α signaling during thymopoiesis in maintaining POT1 expression and telomere integrity, which may shed light on future studies on immune deficiency and lymphomagenesis. Moreover, this DKO mouse may represent a unique model for studying cytokine withdrawal-induced chromosome instability in tumorigenesis.

Materials and Methods

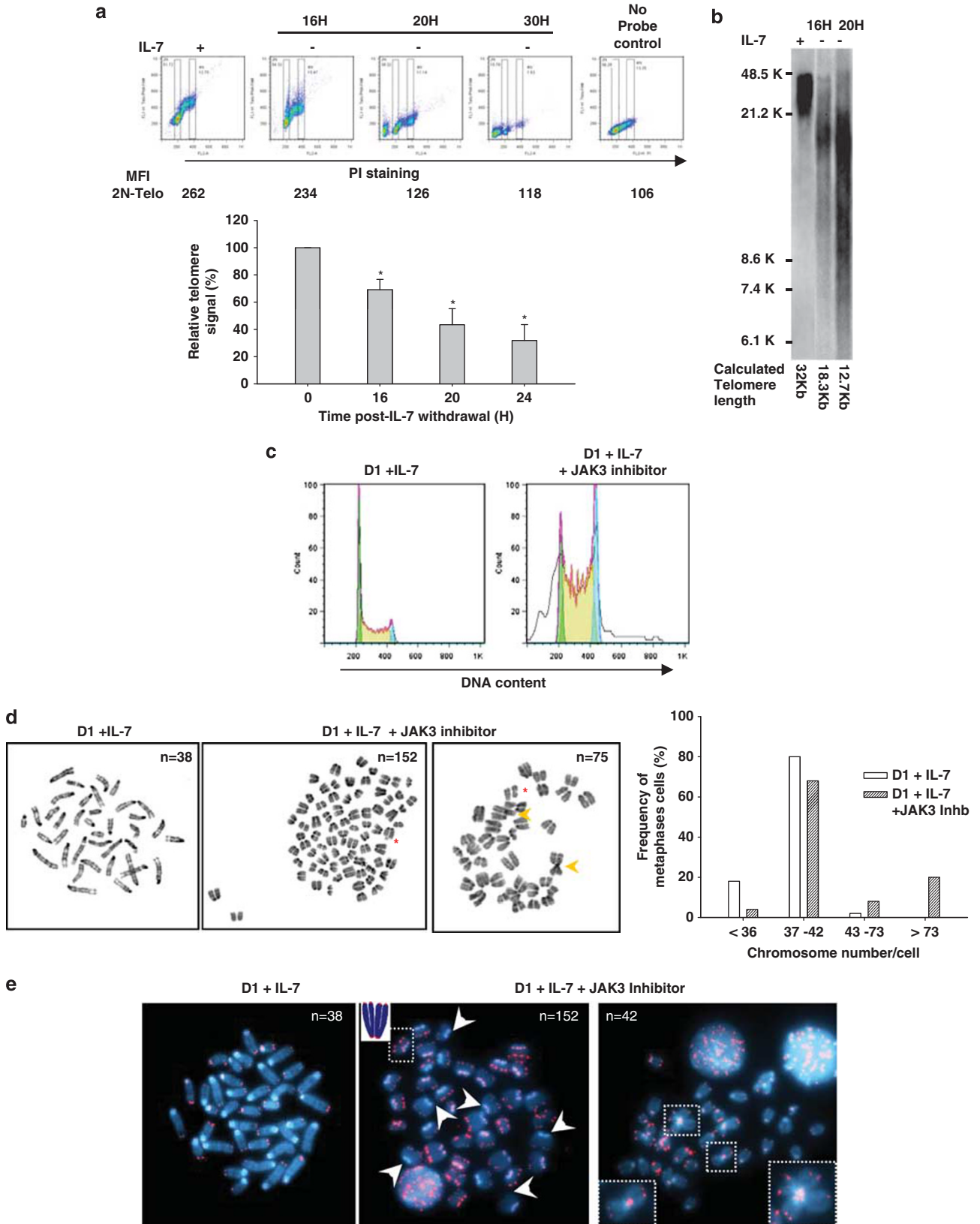
Mice. DKO mice were generated by intercrossing *IL-7R α* ^{nu/nu} (B6.129S7-Il7^{tm1mx/J}) *p53*^{nu/nu} mice for more than five generations. All mice, including *Rag1*^{nu/nu} (B6.129S7-*Rag1*^{tm1Mom/J}), were purchased from the Jackson Laboratories (Bar Harbor, ME, USA). All mice were bred and kept under specific pathogen-free conditions in the animal care facility of LSUHSC following protocols approved by the Institutional Animal Care and Use Committee. Genotypes were confirmed by PCR.

Cell lines and retroviral transduction. The IL-7-dependent thymocyte cell line D1 established from p53 KO mice were maintained in RPMI 1640 supplemented with 10% fetal bovine serum (Sigma, St. Louis, MO, USA), 2 mM L-glutamine, 50 μ M β -mercaptoethanol (Invitrogen, Carlsbad, CA, USA), and 50 μ g/ml murine recombinant IL-7 (PeproTech, Rocky Hill, NJ, USA). The D1 cells were treated with 2 μ M JAK3 inhibitor VI (EMD Biosciences, Darmstadt, Germany) for various durations in the presence of 50 μ g/ml IL-7. D1 or D1Bcl2 cells were transduced with retroviruses pLPCN-MycPOT1a, pLPCN-MycPOT1b (kindly provided by Dr. Titia de Lange), or both and selected with puromycin (5 μ g/ml) in the presence of IL-7 for 7 days.

Figure 5 *IL-7R α* deficiency in the absence of *p53* during T-cell development results in telomere dysfunction and elevated DNA damage signals that co-localize with telomeres. (a and b) Telomeres in the metaphase preparations of thymic lymphomas and pre-malignant thymocytes from DKO and *p53*^{nu/nu} mice were examined via Telo-FISH. (a) Representative Telo-FISH images of thymic lymphomas demonstrate telomere dysfunction in DKO tumor compared with that of *p53*^{nu/nu} tumor. Yellow arrowheads indicate missing telomeres at the site of chromosome fusions, whereas white arrowheads reveal missing telomeres of non-fused chromosomes. (b) Representative Telo-FISH images of fresh pre-malignant DKO and *p53*^{nu/nu} thymocytes demonstrate increased telomere losses (white arrowheads) in DKO thymocytes preceding over tumorigenesis. The frequency of metaphases incurring telomere loss in fresh pre-malignant DKO and *p53*^{nu/nu} thymocytes is summarized (right panel). *n* represents the number of metaphases examined. (c) Fresh thymocytes of all four genotype mice were harvested for telomere hybridization using a FAM-labeled telomere probe followed by propidium iodide staining. The mean fluorescence intensity of telomere signals in cells with identical DNA content (2n) was analyzed via Flow-FISH (left panel) and summarized (right panel). (d) Fresh thymocytes of young WT, *IL-7R α* ^{nu/nu}, DKO, and *p53*^{nu/nu} littermates were stained with anti- γ H2AX antibody to locate DNA damage signals and subsequently hybridized with FAM-conjugated PNA probe. Representative confocal microscopic images demonstrate the co-localization of immunofluorescence stained γ H2AX (red) with telomeres (green) as TIF (yellow) (scale bars = 10 μ m). The frequency of cells containing > 4 TIF/cell among 50 cells of each genotype is presented (right panel). Each experiment is repeated at least three times involving 5–8 tumors for mice of each genotype. (e) IL-7-dependent *p53*^{nu/nu} thymic cells D1Bcl2 cultured in the presence or absence of IL-7 were co-immunostained with rabbit anti- γ H2AX-Alexa568 and mouse anti-53BP1-Alexa647 followed by Telo-FISH hybridization with FAM-labeled PNA probe. Representative confocal microscopic deconvolved single-plan images showing IL-7 withdrawal induced DNA damage signals by both γ H2AX and 53BP1 (pseudo colored red) within the same cell were merged with telomere signals (green) to demonstrate the TIF (yellow). DNA was counterstained with DAPI (blue). Scale bars = 2 μ m. Arrowheads indicate TIFs, whereas enlarged images of TIFs from the dashed boxes are presented to the right as separate panels of DNA damage and telomere signals, as well as merged images

Flow cytometry analysis. All antibodies for FACS analyses were purchased from BD Biosciences (San Jose, CA, USA), unless otherwise specified. Thymocytes and thymic lymphomas were harvested and processed to make single-cell

suspensions for cell-surface marker analysis. Flow cytometric acquisition was performed using a FACSCalibur (BD Biosciences) and analyzed using FlowJo software (Tree Star Inc., Ashland, OR, USA).



Histology and immunofluorescence analyses. Fresh tissues were fixed in methanol-free formaldehyde for H&E and immunofluorescent staining. p53⁺ subpopulation was calculated as the percentage of area covered by p53⁺ cells over that of total thymocytes (DAPI⁺).

Intracellular staining of p53^{ser18}. Fresh thymocytes in single-cell suspension were first stained for cell-surface markers and fixed in cold 70% EtOH at -20°C for 4 h. They were subsequently stained with rabbit anti-p53^{ser18} antibody (100 × dilution; Cell Signaling Technology, Boston, MA, USA) and PE-conjugated goat anti-rabbit antibody in FACS buffer (PBS containing 2 mM EDTA, 2% FBS, and 0.01% sodium azide) in the presence of phosphatase inhibitor

(EMD Chemicals, San Diego, CA, USA) at 4°C. The level of p53^{ser18} signal was determined via FACS.

Tumorigenesis and pathological analyses. Cohorts of 26–36 mice/genotype were observed for tumor development. A portion of the tumors was preserved in buffered zinc formalin fixative (Anatech Ltd, Battle Creek, MI, USA), and sectioned for H&E staining. The other portion of the tumors was dissociated to single-cell suspension for surface marker staining and FACS analysis. H&E sections were viewed by a licensed pathologist to determine the tumor type in reference to their cell-surface marker expression and anatomic location of the tumors.

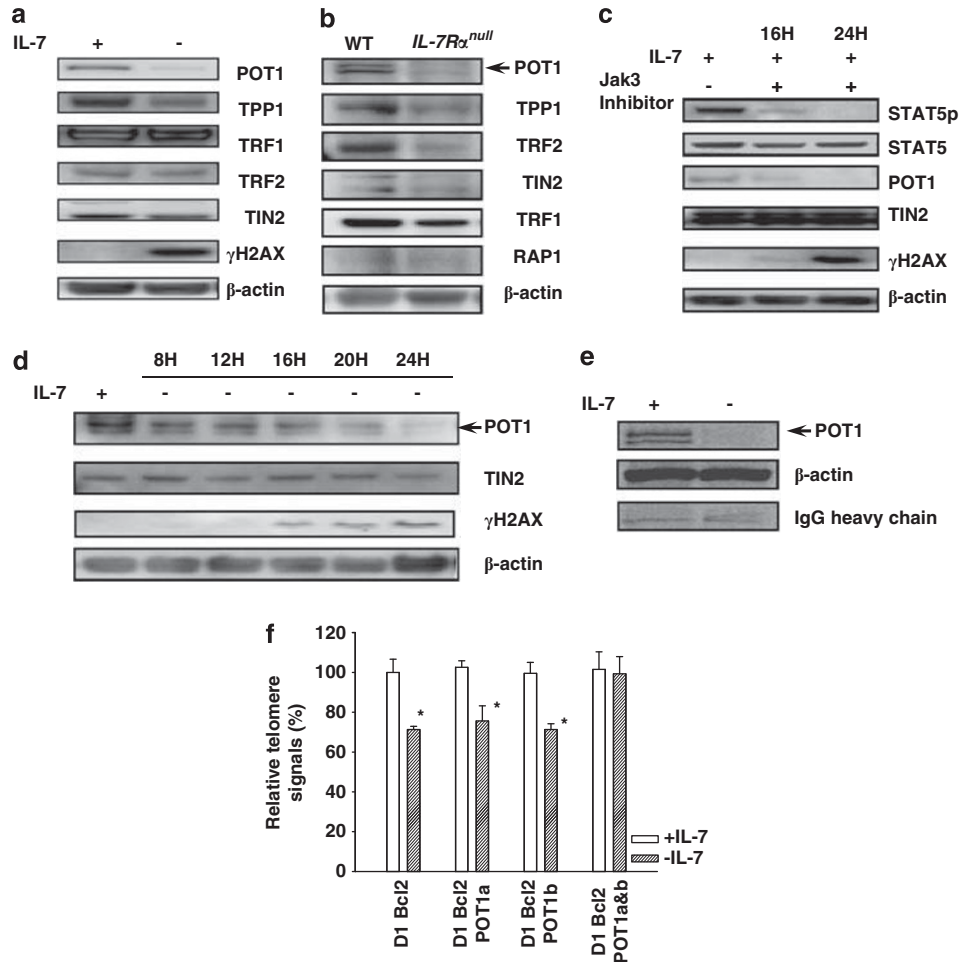


Figure 7 IL-7/IL-7R α signal withdrawal results in diminished protein synthesis of POT1. (a) IL-7-dependent D1 cells were cultured in the presence or absence of IL-7 for 20 h. Alterations in expression level of shelterin subunits and γ H2AX were determined by WB. (b) The expression of POT1 and other subunits of the telomere protective complex shelterin in fresh thymocytes of 4–6-week-old WT and IL-7R α^{null} mice were examined by WB. (c) Kinetics changes in POT1 expression in D1 cells at various durations after IL-7 withdrawal were examined by WB. (d) D1 cells were cultured with 2 μ M of Jak3 inhibitor VI in the presence of IL-7 for various durations. The effects of the Jak3 inhibitor on Stat5 phosphorylation, POT1 expression, and γ H2AX level were examined by WB. (e) D1 cells were cultured in the presence or absence of IL-7 for 12 h followed with 2 h incubation in medium containing ³⁵S-Methionine. Newly synthesized POT1 or β -actin proteins incorporated with ³⁵S-Methionine were immunoprecipitated with antibodies against POT1 or β -actin and were subjected to electrophoresis and autoradiography. All experiments were repeated at least three times with similar results. (f) D1Bcl2 cells retrovirally transduced with POT1a or POT1b, or both POT1a and POT1b were selected by puromycin for 7 days and subjected to IL-7 withdrawal. At 20 h after IL-7 removal, their telomere hybridization signal was determined via Flow-FISH and compared with those cultured in the present of IL-7. Data is presented as mean \pm s.e. of three independent experiments

Figure 6 Blockade of IL-7/IL7R α signaling by a Jak3 inhibitor in an IL-7-dependent p53^{null} thymic cell line recapitulated chromosome and telomere anomalies observed in DKO lymphomas. (a) IL-7-dependent p53^{null} D1 cells were cultured in the presence or absence of IL-7 for various durations and the alteration in their telomere signals were examined via Flow-FISH and summarized at the bottom. (b) Telomere attrition in D1 cells following IL-7 withdrawal was determined via a Southern blot based analysis of TRF assay. (c–e) The effect of the JAK3 inhibitor on inducing chromosome and telomere anomalies in D1 cells 40 h post treatment was examined via FACS (c), G-band karyotyping (d), and Telo-FISH (e). Red asterisks indicate chromosome breaks; yellow arrowheads, chromosome fusions; and white arrow heads, telomere dysfunction; inserts demonstrate chromosome amplifications and fusions. Representative of at least three independent experiments

Western blotting. Fresh thymocytes or cultured D1 cells were lysed in RIPA buffer containing phosphatase inhibitors and protease inhibitors (EMD Chemicals). Cell lysate containing 20–100 μ g protein was loaded onto the NuPAGE 4–12% Bis-Tris or 7% Tris-Acetate gel (Invitrogen), separated by electrophoresis, transferred to the PVDF membrane (Invitrogen), and blotted with antibodies against specific proteins. The primary antibodies are p53 (CM5; Novocastra, Newcastle upon Tyne, UK); p53Ser¹⁵, p53Ser²⁰, puma, p21, γ H2AX, Stat5-Tyr⁶⁹⁴, Stat5, and repressor activator protein 1 (Cell Signaling); Vinculin and TRF2 (Santa Cruz, Santa Cruz, CA, USA); β -actin (Sigma); and POT1, TIN2, and TRF1 (Abcam, Cambridge, MA, USA).

Metaphase preparation and karyotyping. Primary thymic lymphomas from p53^{null} and DKO mice were expanded in the presence of recombinant IL-2 (20 U/ml) and treated with 100 ng/ml Colcemid (Invitrogen) for 1 h before harvesting for metaphase preparation. For metaphase preparation of fresh thymocytes, cells from 6–8-week-old mice were harvested 2 h after they were treated i.p. with Colcemid at 30 μ g/kg body weight. Metaphase preparations were performed following standard procedures.³⁹ Karyotypes of metaphase images were captured using an Applied Imaging Model ER-3339 cooled CCD camera (Applied Spectral Imaging Inc., Vista, CA, USA) mounted on top of a Nikon Eclipse E400 with CytoVision version 3.1 image-capture software (Applied Spectral Imaging). Telomere *in situ* hybridization and SKY analyses were performed using Cy3-labeled telomere PNA (CCCTAA)₃ probe (Panagene Inc., Daejeon, Korea) and 20-color mouse SKY paint kit (ASI), respectively, following standard procedures and manufacturer's instructions.³⁹ SKY images were acquired using a SD301 SpectraCubeTM system (ASI) mounted on top of an epifluorescence microscope Axioplan 2 (Zeiss, Oberkochen, Germany). Images were analyzed using Spectral Imaging 4.0 acquisition software (ASI). G-banding was simulated by electronic inversion of DAPI counterstaining.

IF-FISH. IF-FISH was performed with primary thymocytes or established cell lines. Cells in suspension were fixed in 2% paraformaldehyde at RT for 10 min, cytospun onto coated microscope slides (Shandon, Pittsburgh, PA, USA) followed by acetone treatment at -20°C for 5 min, and 30 min incubation with blocking solution (1% BSA and 5% goat serum in PBS). Primary antibodies, γ H2AX (mouse monoclonal, JBW301; Millipore, Billerica, MA, USA) and 53BP1 (rabbit polyclonal, 100-304, Novus Biologicals, Littleton, CO, USA) were incubated in blocking solution at RT for 2 h, followed by 30 min incubation with Alexa-568-labeled goat anti-rabbit and Alexa-647-labeled goat anti-mouse antibodies (Invitrogen). The slides were completely dehydrated by pass through 75%, 95%, and 100% ethanol and air-dried for 5 min. Telomere *in situ* hybridization was performed with 140 nM FAM-labeled telomere PNA (CCCTAA)₃ probe (Panagene Inc.) in hybridization buffer (70% formamide, 20 mM Tris-HCl, 10 mM Na₂HPO₄, and 10 mM NaCl) at 80 $^{\circ}\text{C}$ for 5 min, followed by 1 h hybridization in dark at RT. The slides were washed with PBS containing 0.1% Tween-20 at 57 $^{\circ}\text{C}$ for 20 min, followed by 2 \times SSC containing 0.1% Tween 20 at RT for 5 min, DAPI counterstained and mounted in ProLong Gold (Invitrogen).

Flow-FISH. Flow cytometry-based analysis of telomere signal (Flow-FISH) was performed following a standard protocol⁴⁰ with slight modification. Briefly, cells were incubated with 28 nM FAM-labeled telomere PNA (CCCTAA)₃ probe in hybridization buffer at RT for 10 min, followed by a 10 min incubation at 87 $^{\circ}\text{C}$, and a 90-min incubation at RT in dark. After two washes with PBS containing 0.1% Tween-20 and two washes with 2 \times SSC containing 0.1% Tween 20, they were incubated in 350 μ l of RNase/propidium iodide-staining buffer (BD Biosciences) at RT for 15 min and used for FACS analysis. FAM-labeled telomere signal was detected at FL1 and cells with the same DNA content were compared.

TRF assay. A Southern blot-based TRF analysis was performed using a TeloTAGGG telomere Length Assay kit (Roche, Basel, Switzerland) as per manufacturer's instruction. Briefly, 2 μ g of genomic DNA harvested from D1 cells cultured in the presence or absence was digested with Hinf I and Rsa I at 37 $^{\circ}\text{C}$ for 4 h and electrophoresed in 0.7% agarose gel at 25 V for 20 h. The gel was then treated with 0.25 N HCl for 30 min, denatured with 0.5 N NaOH for 20 min, and transferred onto Hybond-N⁺ membrane (GE Healthcare, Waukesha, WI, USA) with 0.4 N NaOH for 4 h. The membrane was subsequently hybridized with DIG-labeled telomere probe at 42 $^{\circ}\text{C}$ for 3 h, followed by two washes with 2 \times SSC containing 0.1% SDS at RT and 0.2 \times SSC containing 0.1% SDS at 50 $^{\circ}\text{C}$ for 15 min each. The telomere signal was revealed by incubating the membrane with AP-conjugated anti-DIG antibody, followed by AP substrate addition, and acquired via a BioRad VersaDoc imaging system. The telomere length of each sample was determined by

first measuring the signal density (OD) for each of the 35–40 equally sized squares over the entire gel length and calculated as $\text{TRF} = \Sigma(\text{OD}_i) / \Sigma(\text{OD}_i / L_i)$, where OD_i is the signal density of each individual square and L_i is the length of the TRF at the position i.

Analyses of protein synthesis. To examine *de novo* protein synthesis of POT1 upon IL-7 withdrawal, D1 cells cultured in the absence or presence of IL-7 for 12 h were transferred to Methionine-free RPMI (Invitrogen) medium for 30 min followed by pulsing with ³⁵S Methionine at 20 mCi/ml (1175 Ci/mmol, PerkinElmer, Waltham, MA, USA) for 2 h. Cell lysate containing 100 μ g of the total protein was used for IP with 3 μ g of rabbit anti-POT1 antibody (Abcam) and Protein G Agarose beads at 4 $^{\circ}\text{C}$ o/n. Eluted proteins were separated via electrophoresis with an 8% Tris-Glycine NuPAGE gel (Invitrogen), transferred onto PVDF membrane, and ³⁵S Methionine-labeled proteins were detected by exposing to a Biomax MR film.

Statistical analysis. The differences in cell survival and gene expression between different samples and/or treatments were analyzed via two-tailed Student's *t*-tests using SigmaPlot (Systat Software Inc., Chicago, IL, USA). Statistical significance was set at $P < 0.05$, unless otherwise stated in the text.

Conflict of interest

The authors declare no conflict of interest.

Acknowledgements. We thank Drs. Alistair Ramsay, Wanguo Liu, Jay K Kolls, and Drew Pardoll for constructive suggestions; Ms. Heidi Davis for editorial assistance; Drs. Beatriz Finkel-Jimenez, Sandra Burkett, Marilyn Li, and Kong Chen for technical assistance; and Ms. Yunping Huang for animal breeding. This work is supported in part by funds from the LGTRC, LCRC, NIH grants to YC (CA112065 and P20RR021970) and TI (P20RR020152).

- Mazzucchelli R, Durum SK. Interleukin-7 receptor expression: intelligent design. *Nat Rev Immunol* 2007; **7**: 144–154.
- Buckley RH. Molecular defects in human severe combined immunodeficiency and approaches to immune reconstitution. *Annu Rev Immunol* 2004; **22**: 625–655.
- Puel A, Ziegler SF, Buckley RH, Leonard WJ. Defective IL7R expression in T(-)B(+)NK(+) severe combined immunodeficiency. *Nat Genet* 1998; **20**: 394–397.
- Peschon JJ, Morrissey PJ, Grabstein KH, Ramsdell FJ, Maraskovsky E, Gliniak BC et al. Early lymphocyte expansion is severely impaired in interleukin 7 receptor-deficient mice. *J Exp Med* 1994; **180**: 1955–1960.
- Akashi K, Kondo M, von Freeden-Jeffry U, Murray R, Weissman IL. Bcl-2 rescues T lymphopoiesis in interleukin-7 receptor-deficient mice. *Cell* 1997; **89**: 1033–1041.
- Khaled AR, Li WQ, Huang J, Fry TJ, Khaled AS, Mackall CL et al. Bax deficiency partially corrects interleukin-7 receptor alpha deficiency. *Immunity* 2002; **17**: 561–573.
- Maraskovsky E, O'Reilly LA, Teepe M, Corcoran LM, Peschon JJ, Strasser A. Bcl-2 can rescue T lymphocyte development in interleukin-7 receptor-deficient mice but not in mutant rag-1/- mice. *Cell* 1997; **89**: 1011–1019.
- Levine AJ. p53, the cellular gatekeeper for growth and division. *Cell* 1997; **88**: 323–331.
- Guidos CJ, Williams CJ, Grandal I, Knowles G, Huang MT, Danska JS. V(D)J recombination activates a p53-dependent DNA damage checkpoint in scid lymphocyte precursors. *Genes Dev* 1996; **10**: 2038–2054.
- Green DR, Schuler M. T cell development: some cells get all the breaks. *Nat Immunol* 2000; **1**: 15–17.
- Mak TW, Hakem A, McPherson JP, Shehabeldin A, Zabolocki E, Migon E et al. Bcl-2 required for T cell lineage development but not TCR loci rearrangement. *Nat Immunol* 2000; **1**: 77–82.
- Aparicio S, Eaves CJ. p53: a new kingpin in the stem cell arena. *Cell* 2009; **138**: 1060–1062.
- Levine AJ, Oren M. The first 30 years of p53: growing ever more complex. *Nat Rev Cancer* 2009; **9**: 749–758.
- Zheng SJ, Lamhamedi-Cherradi SE, Wang P, Xu L, Chen YH. Tumor suppressor p53 inhibits autoimmune inflammation and macrophage function. *Diabetes* 2005; **54**: 1423–1428.
- Zhang S, Zheng M, Kibe R, Huang Y, Marrero L, Warren S et al. Trp53 negatively regulates autoimmunity via the STAT3-Th17 axis. *FASEB J* 2011; **25**: 2387–2398.
- Chao C, Herr D, Chun J, Xu Y. Ser18 and 23 phosphorylation is required for p53-dependent apoptosis and tumor suppression. *EMBO J* 2006; **25**: 2615–2622.
- Jacks T, Remington L, Williams BO, Schmitt EM, Halachmi S, Bronson RT et al. Tumor spectrum analysis in p53-mutant mice. *Curr Biol* 1994; **4**: 1–7.
- Mills KD, Ferguson DO, Alt FW. The role of DNA breaks in genomic instability and tumorigenesis. *Immunol Rev* 2003; **194**: 77–95.

19. Feldser DM, Hackett JA, Greider CW. Telomere dysfunction and the initiation of genome instability. *Nat Rev Cancer* 2003; **3**: 623–627.
20. Haines BB, Ryu CJ, Chang S, Protopopov A, Luch A, Kang YH *et al*. Block of T cell development in P53-deficient mice accelerates development of lymphomas with characteristic RAG-dependent cytogenetic alterations. *Cancer Cell* 2006; **9**: 109–120.
21. Liu G, Parant JM, Lang G, Chau P, Chavez-Reyes A, El-Naggar AK *et al*. Chromosome stability, in the absence of apoptosis, is critical for suppression of tumorigenesis in Trp53 mutant mice. *Nat Genet* 2004; **36**: 63–68.
22. Williams ES, Klingler R, Ponnaiya B, Hardt T, Schrock E, Lees-Miller SP *et al*. Telomere dysfunction and DNA-PKcs deficiency: characterization and consequence. *Cancer Res* 2009; **69**: 2100–2107.
23. Chin L, Artandi SE, Shen Q, Tam A, Lee SL, Gottlieb GJ *et al*. p53 deficiency rescues the adverse effects of telomere loss and cooperates with telomere dysfunction to accelerate carcinogenesis. *Cell* 1999; **97**: 527–538.
24. Goytisolo FA, Samper E, Edmonson S, Taccioli GE, Blasco MA. The absence of the dna-dependent protein kinase catalytic subunit in mice results in anaphase bridges and in increased telomeric fusions with normal telomere length and G-strand overhang. *Mol Cell Biol* 2001; **21**: 3642–3651.
25. d'Adda di Fagagna F, Reaper PM, Clay-Farrace L, Fiegler H, Carr P, Von Zglinicki T *et al*. A DNA damage checkpoint response in telomere-initiated senescence. *Nature* 2003; **426**: 194–198.
26. Martinez P, Blasco MA. Telomeric and extra-telomeric roles for telomerase and the telomere-binding proteins. *Nat Rev Cancer* 2011; **11**: 161–176.
27. Thanasoula M, Escandell JM, Martinez P, Badie S, Munoz P, Blasco MA *et al*. p53 prevents entry into mitosis with uncapped telomeres. *Curr Biol* 2010; **20**: 521–526.
28. Takai H, Smogorzewska A, de Lange T. DNA damage foci at dysfunctional telomeres. *Curr Biol* 2003; **13**: 1549–1556.
29. Kim K, Khaled AR, Reynolds D, Young HA, Lee CK, Durum SK. Characterization of an interleukin-7-dependent thymic cell line derived from a p53(-/-) mouse. *J Immunol Methods* 2003; **274**: 177–184.
30. Li WQ, Jiang Q, Aleem E, Kaldis P, Khaled AR, Durum SK. IL-7 promotes T cell proliferation through destabilization of p27Kip1. *J Exp Med* 2006; **203**: 573–582.
31. Baumann P, Cech TR. Pot1, the putative telomere end-binding protein in fission yeast and humans. *Science* 2001; **292**: 1171–1175.
32. Hockemeyer D, Daniels JP, Takai H, de Lange T. Recent expansion of the telomeric complex in rodents: Two distinct POT1 proteins protect mouse telomeres. *Cell* 2006; **126**: 63–77.
33. Davoli T, Denchi EL, de Lange T. Persistent telomere damage induces bypass of mitosis and tetraploidy. *Cell* 2010; **141**: 81–93.
34. Reiterer G, Yen A. Inhibition of the janus kinase family increases extracellular signal-regulated kinase 1/2 phosphorylation and causes endoreduplication. *Cancer Res* 2006; **66**: 9083–9089.
35. Shochat C, Tal N, Bandapalli OR, Palmi C, Ganmore I, Te Kronnie G *et al*. Gain-of-function mutations in interleukin-7 receptor- α (IL7R) in childhood acute lymphoblastic leukemias. *J Exp Med* 2011; **208**: 901–908.
36. Zenatti PP, Ribeiro D, Li W, Zuurbier L, Silva MC, Paganin M *et al*. Oncogenic IL7R gain-of-function mutations in childhood T-cell acute lymphoblastic leukemia. *Nat Genet* 2011; **43**: 932–939.
37. Michalak EM, Vandenberg CJ, Delbridge AR, Wu L, Scott CL, Adams JM *et al*. Apoptosis-promoted tumorigenesis: gamma-irradiation-induced thymic lymphomagenesis requires Puma-driven leukocyte death. *Genes Dev* 2010; **24**: 1608–1613.
38. Labi V, Erlacher M, Krumschnabel G, Manzl C, Tzankov A, Pinon J *et al*. Apoptosis of leukocytes triggered by acute DNA damage promotes lymphoma formation. *Genes Dev* 2010; **24**: 1602–1607.
39. Padilla-Nash HM, Barenboim-Stapleton L, Diflippantonio MJ, Ried T. Spectral karyotyping analysis of human and mouse chromosomes. *Nat Protoc* 2006; **1**: 3129–3142.
40. Baerlocher GM, Vulto I, de Jong G, Lansdorp PM. Flow cytometry and FISH to measure the average length of telomeres (flow FISH). *Nat Protoc* 2006; **1**: 2365–2376.

Supplementary Information accompanies the paper on Cell Death and Differentiation website (<http://www.nature.com/cdd>)